Supporting Information

Microwave-assisted synthesis of Co-Free Li[Li$_{0.2}$Ni$_{0.2}$Mn$_{0.6}$]O$_2$ cathodes with spinel-layered coherent structure for high-power Li-ion batteries

Shenggui Wang[1,2,3,*], Jinniu Chen[4], Tian Zhao[4], Xiaoxia Yang[4], Lang Qiu[3], Zhonghua Wu[5], Yang Song[3], Xiaodong Guo[3,*] and Kun Yu[1,*]

[1] School of Materials Science and Engineering, Central South University, Changsha 410083, China. Email: w-sh-g@163.com; yukun2010@csu.edu.cn.

[2] Kunming Branch of the 705 Research lnstitute, China State Shipbuilding Corporation Limited, Kunming 650032, China.

[3] School of Chemical Engineering, Sichuan University, No. 24 South Section 1, Yihuan Road, 610065, Chengdu, China. Email: xiaodong2009@scu.edu.cn.

[4] School of Chemical Engineering and Technology, Xi'an Jiaotong University, No.28, West Xianning Road, Xi'an, Shaanxi 710049, China.

[5] Beijing Synchrotron Radiation Facility, Institute of High Energy Physics, Chinese Academy of Sciences, Beijing, China.

1. EXPERIMENTAL SECTION

1.1 Material preparation

The precursor was synthesized by a hydroxide co-precipitation method. Firstly, a 2 M aqueous solution of stoichiometrically mixed $NiSO_4 \cdot 6H_2O$ and $MnSO_4 \cdot H_2O$ (molar ratio of Ni and Mn is 1:3) was added into a continuous stirred tank reactor (CSTR) at the feeding rate of 2 ml min^{-1}. At the same time, 4 M precipitant solution (NaOH) and a desired amount of $NH_3 \cdot H_2O$ solution (complexing agent) were added into the reactor. The pH value (11.3 ± 0.3), temperature (52 ± 2 °C), and stirring speed (500 rpm) were carefully controlled, and the whole process was carried out under N_2 atmosphere. The co-precipitated particles were filtered, washed with distilled water for several times to remove the Na^+ and SO_4^{2-} ions and dried at 100 °C overnight.

In addition, to investigate the real structure of the LLNMO-LS. The prepared precursor for $Li[Li_{0.2}Ni_{0.2}Mn_{0.6}]O_2$ materials was totally mixed with 5 % excess of Li_2CO_3. The obtained mixture was heated at 700°C, with the heating rate of 30 °C /min, for 1 hours through a microwave chamber with air atmosphere to obtain the final materials, which are marked as LLNMO-LS.

For comparison, the layered $Li[Li_{0.2}Ni_{0.2}Mn_{0.6}]O_2$ (LLNMO-L) cathode material was prepared by annealing a mixture of obtained precursor and Li_2CO_3 at 850 °C for 12 hours in air via a traditional furnace, the molar ratio of transitional metal and lithium in the mixture is 1:1.6.

1.2. Material Characterization

The crystalline structural evolution of LLNMO-LS and LLNMO-L was characterized by high-resolution synchrotron-based XRD patterns (SXRD). The unit cell parameters of LLNMO-LS and LLNMO-L were refined to the SXRD patterns using Fullprof software. Particle morphology and structure were measured by scanning electron microscopy (GeminiSEM 500). An aberration-corrected scanning transmission electron microscope (STEM, Talos F200X) equipped with double probe aberration-correctors was employed to investigate the structure at the atomic scale. All of the microscopes were operated at 200 kV. The convergence semi-angle for STEM imaging

was approximately 25 mrad, while the collection semi-angle was 70–250 mrad for Z-contrast high angle annular dark-field (HAADF) scanning transmission electron microscopy imaging. The STEM-EDX mapping results were obtained using a NSS software. Electron energy loss spectroscopy (EELS) spectrum imaging data cubes were acquired with a probe convergence angle of 30 mrad and a probe current of 80 pA. X-ray absorption spectroscopy (XAS) measurements were performed at the 4B9A beamline in Beijing Synchrotron Radiation Facility (BSRF).

Brunauer–Emmett–Teller (BET, Quadrasorb SI) nitrogen sorption isotherms were utilized to analyse the pore size distribution of the samples. The elemental concentration of the particles was detected by inductively coupled plasma/optical emission spectrometry (ICP-OES) measurements. The electronic structure of the materials was determined by X-ray photoelectron spectroscopy (XPS) and the curve fittings were performed with the XPS PEAK program. Transmission electron microscopy (TEM, JEM-2100) were used to investigate the micro-structure of fatigued cathode materials. The structural evolution of LLNMO-LS materials upon (de)lithiation was investigated by powder X-ray diffractometry Lab-X, XRD-6100 with Cu Kα radiation source in the 2θ range of 10-80˚ and an exposure time of 10 min per pattern. The lattice parameters were refined by using the Rietveld method with the program FullProf.

1.3. Electrochemical measurements

The ccathode of the battery is composed of 80 wt.% positive electrode material, 13 wt.% acetylene black, 7 wt.% PVDF (polyvinylidene fluoride), and moderate amount of NMP (N-methyl-2-pyrrolidone). The mixture was ball milled for 16 minutes and then spread into a uniform film on an Al foil, subsequently vacuum-dried for 12 h at 120 °C to remove NMP. The loading mass of the positive material in the electrode was 4 ± 0.5 mg cm^{-2}. The coin cells were assembled with positive electrode, separator (Celgard 2325), lithium plate and 40 μL electrolyte (1M LiPF$_6$ dissolved in ethylene carbonate and dimethyl carbonate (1:1vol)) using CR2032 cases in a glove box. The coin cells were tested between 2.0 and 4.8 V (versus Li/Li$^+$).
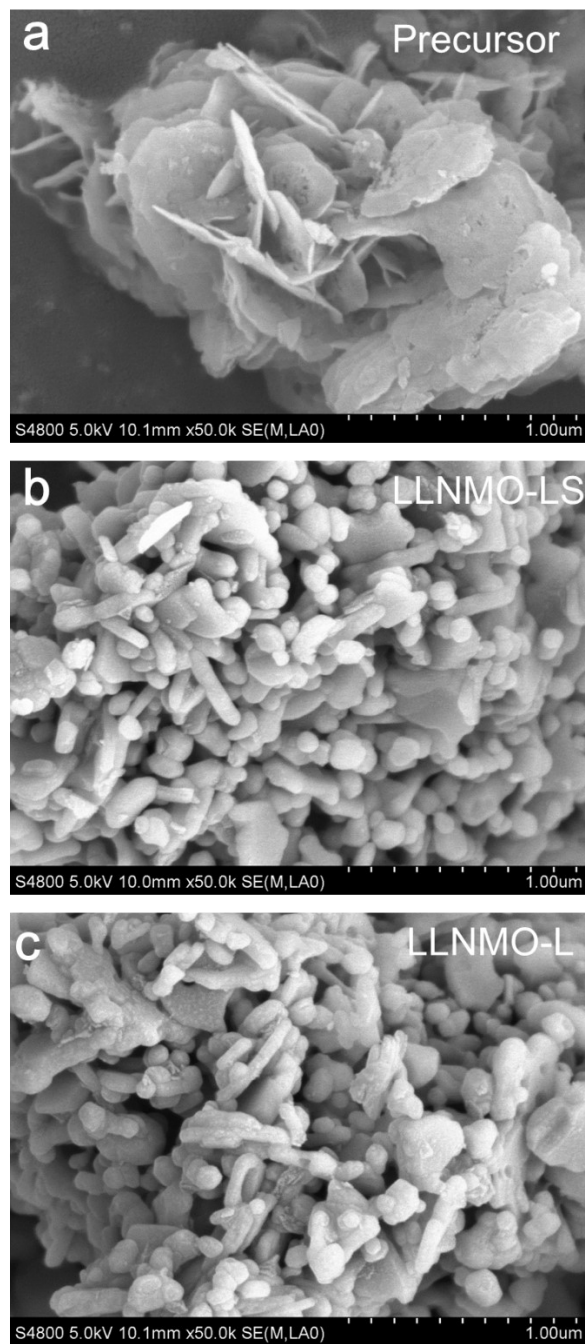
2. Additional results

Figure S1. SEM images of the (**a**) precursor, (**b**) LLNMO-LS and (**c**) LLNMO-L.
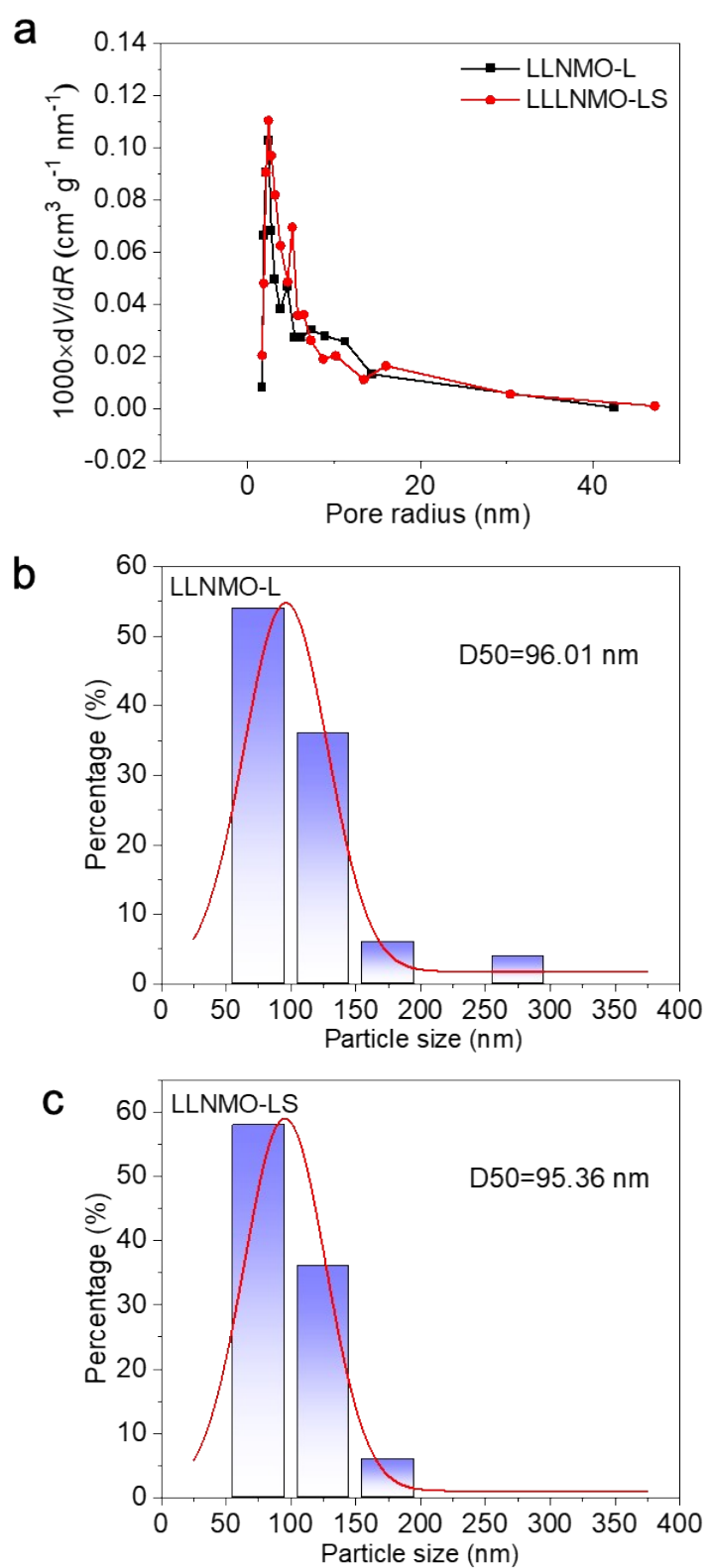
Figure S2. (**a**) The porosity of LLNMO-L and LLNMO-LS; the primary particle size

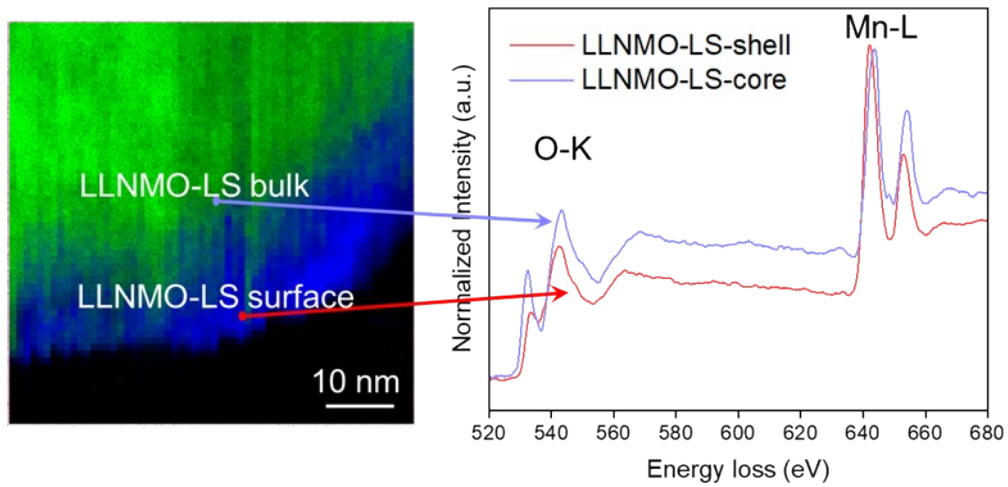distribution of (**b**) LLNMO-L and (**c**) LLNMO-LS.

Figure S3. (**a**) Mn L-edge chemical shift mapping, normalized EEL spectra; (**b**) O K-edge/Mn L-edge on core and shell of LLNMO-LS.

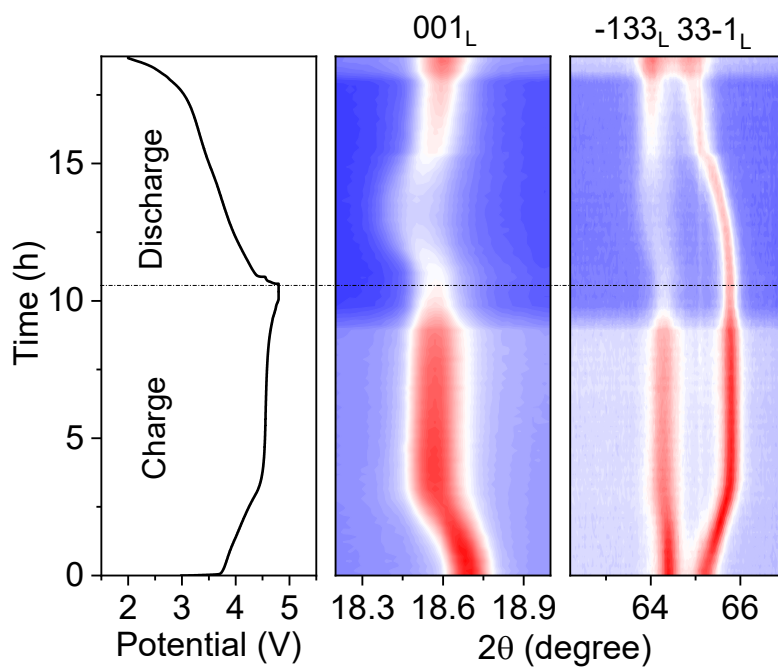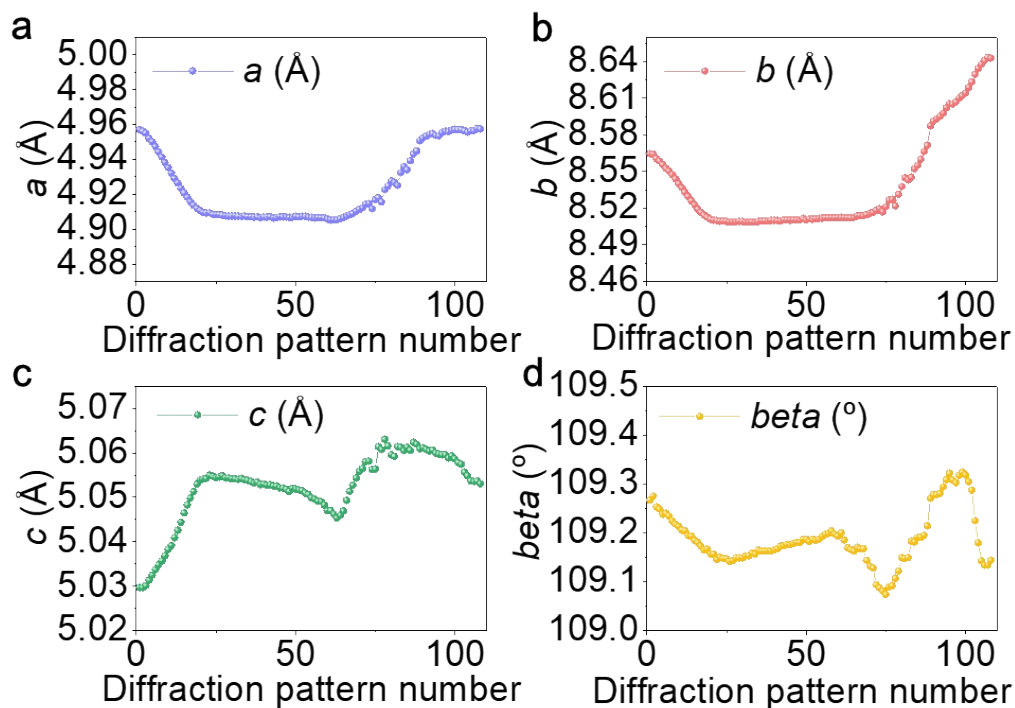**Figure S4.** *In situ* XRD patterns of LLNMO-LS electrode during the first cycle.

Figure S5. Changes of lattice parameters (*a, b, c,* and *beta*) for LLNMO-LS electrode during cycling.

During the initial charging process, the 001 and -133 reflections of LLNMO-LS progressively shifted towards lower scattering angles as the potential climbed to around 4.5 V. Upon charging the LLNMO-LS electrode to 4.8 V, they marginally reverted to a higher 2θ angle. Meanwhile, the 33-1 reflection moved towards higher scattering angles at 4.5 V and remained nearly unchanged until further charging to 4.8 V (see Figure S5). As the discharge process ensued, all reflections tended to revert back to their primary positions.

From the open circuit voltage to 4.5 V, the *c* parameter of the LLNMO-LS electrode steadily increased. This rise is attributed to the heightened electrostatic repulsion force

within the oxygen framework, triggered by the decrease in the number of Li ions in the Li layer. Consequently, this led to an increase in the average distance between the TM-TM crystal planes. Simultaneously, both the *a* and *b* parameters of the LLNMO-LS electrode decreased. This contraction is associated with the reduction in the distance within the average TM-TM plane, believed to result from the oxidation of transition metal ions. Upon further elevation of the potential to 4.8 V, a slight decrease in the *c* parameter was noted, while parameters a and b remained relatively unchanged.

During the initial discharge, the lattice parameters of the LLNMO-LS electrode exhibit a tendency to revert to their original values, yet they don't fully reach their initial state.
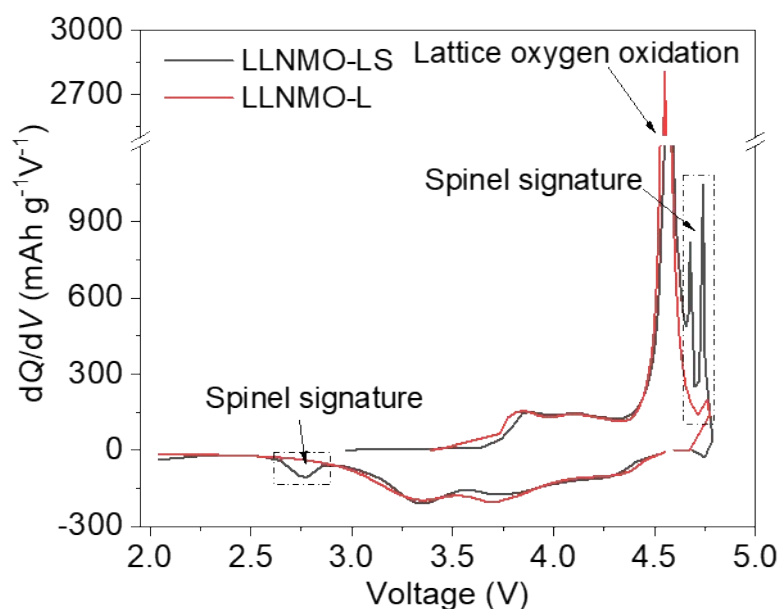
.

Figure S6. The differential capacity (dQ/dV) of LLNMO-LS and LLNMO-L cathodes during the first cycle.
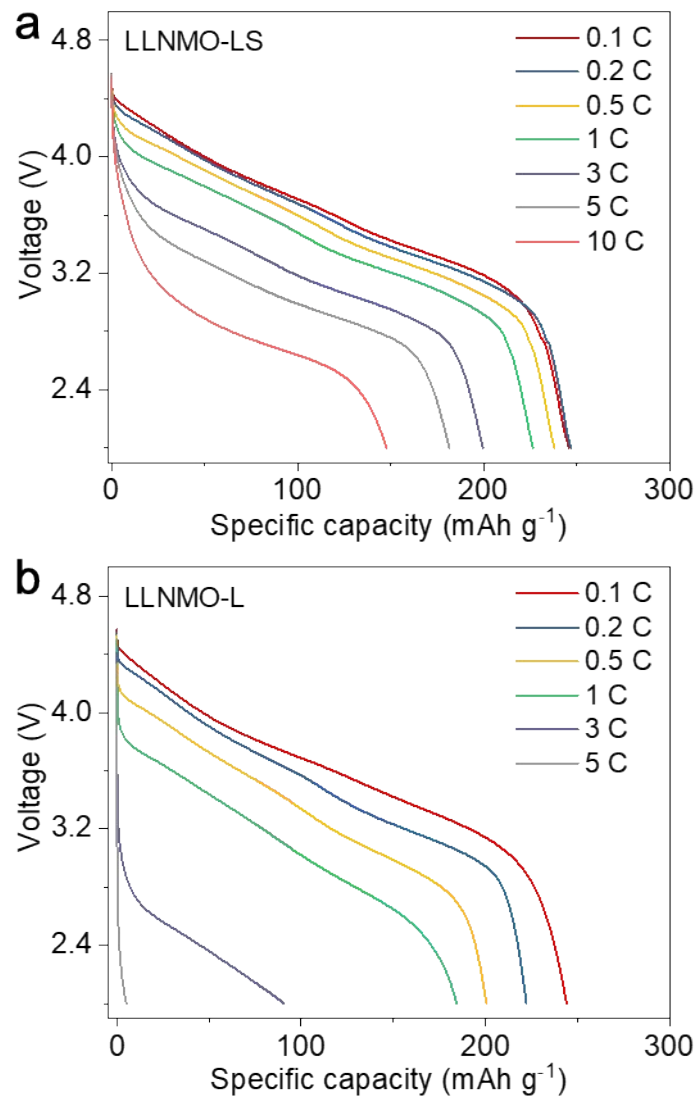
Figure S7. The discharge curves of (**a**) LLNMO-LS and (**b**) LLNMO-L cathodes at various rates within 2.0-4.8 V.

EIS was conducted to analyze the Li$^+$ diffusion kinetics of LLNMO-LS and LLNMO-L. As shown in **Figure 3d**, the EIS curves of the two cathodes are composed of a semicircle in high-to-intermediate frequency region and an inclined line in low-frequency region. The inset of **Figure 3** provides the corresponding equivalent circuit. The lithium-ion diffusion coefficients for LLNMO-LS and LLNMO-L were calculated

aaccording to the following equation:

$$D_{Li^+} = R^2T^2/2n^4F^4A^2\sigma^2c^2$$

where D represents lithium-ion diffusion coefficient, R is the gas constant, T is the absolute temperature, n is the number of electrons transferred per molecule during the electrochemical reactions, F is Faraday constant, A denotes the electrode area, σ represents the Warburg impedance coefficient and c is molar concentration of Li^+. As exhibited in **Table S3**, the higher R_{ct} (189 Ω) and lower D_{Li^+} (2.08×10^{-13} cm^{-2} s^{-1}) of LLNMO-L electrode compared to those of LLNMO-LS electrode (146 Ω, 9.66×10^{-13} cm^{-2} s^{-1}) indicate sluggish Li-ion transport kinetics in LLNMO-L electrode.

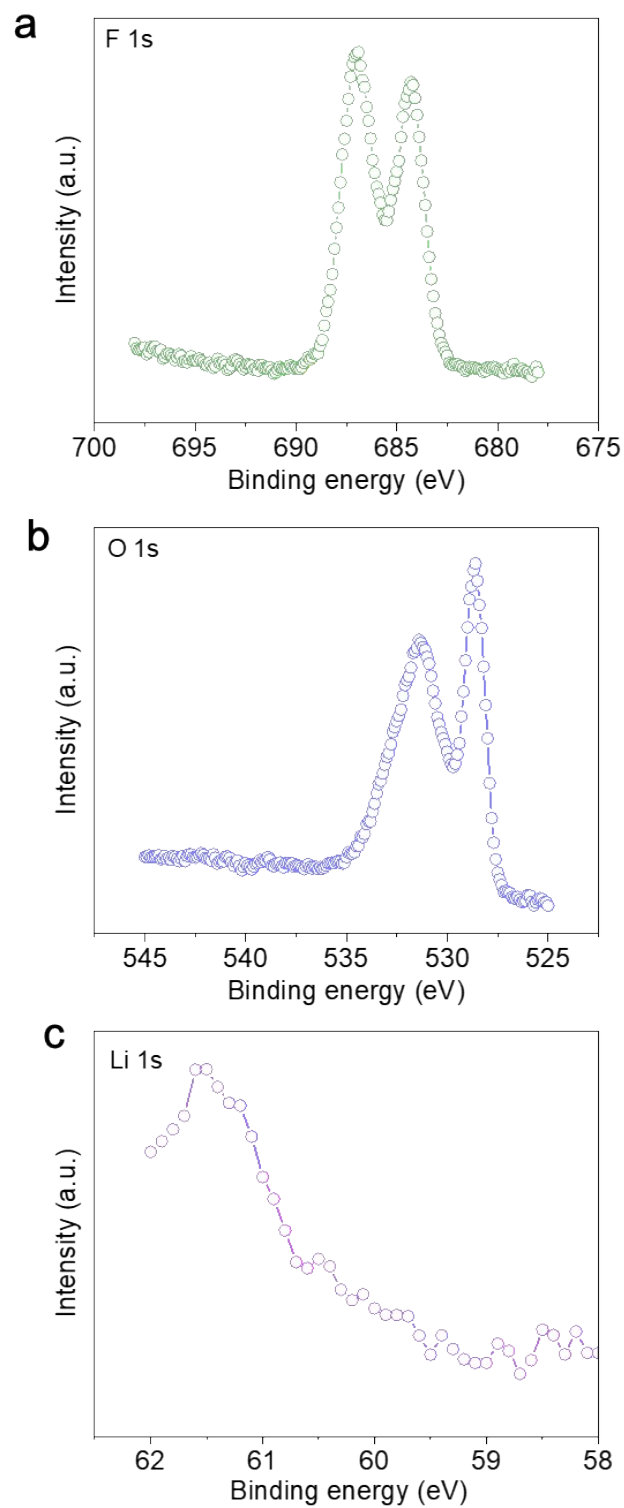**Figure S8.** High-resolution XPS spectra of (**a**) F 1s, (**b**) O 1s and (**c**) Li 1s of fatigued
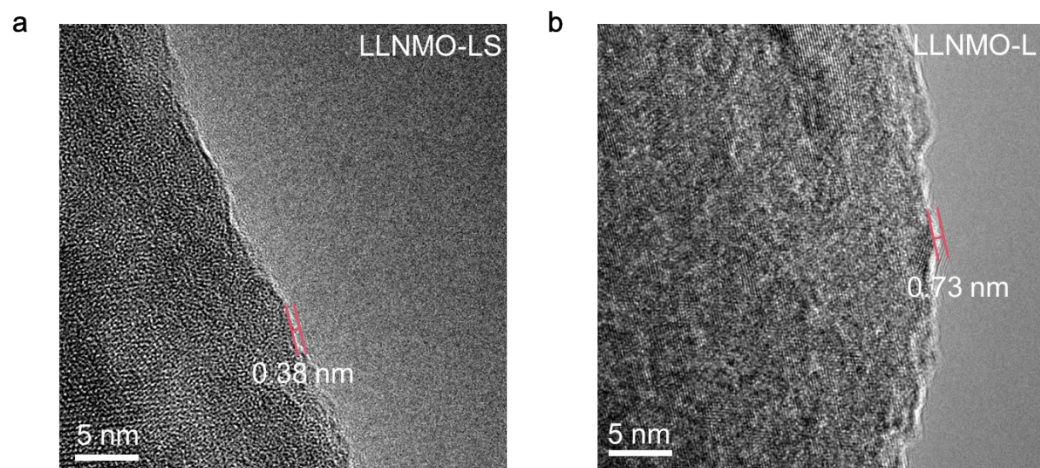
LLNMO-LS cathode.

Figure S9. HAADF-STEM image of cycled (**a**) LLNMO-LS and (**b**) LLNMO-L in the discharged state.

Table S1. Element content of LLNMO-L and LLNMO-LS.

Sample	Li	Ni	Mn
LLNMO-L	1.203	0.205	0.602
LLNMO-LS	1.201	0.202	0.604

Table S2. Crystallographic parameters of LLNMO-L.

Cell parameters

Space group: $C2/m$, a = 4.9642(2) Å b = 8.5734(3) Å, , c = 5.0363(5) Å, beta = 109.2870(5)°,

V = 202.3183(7) Å^3,

Atomic positions

Name	site	x	y	z	Fract
Li1	2c	0.000	0.000	0.500	1.000
Li2	4h	0.000	0.695	0.500	0.944
Ni2	4h	0.000	0.695	0.500	0.054
Ni1	2b	0.000	0.500	0.000	0.212
Li3	2b	0.000	0.500	0.000	0.416
Mn2	2b	0.000	0.500	0.000	0.380
Mn1	4g	0.000	0.174	0.000	0.710
Ni3	4g	0.000	0.173	0.000	0.140
Li4	4g	0.000	0.173	0.000	0.149
O1	4i	0.216	0.000	0.223	1.000
O2	8j	0.250	0.332	0.228	1.000

Refinement parameters

R_{wp}= 3.12 %, R_p= 1. 93 %, χ^2: 1.89

Note: Fract is the fractional occupancy of the atom on this site.

Table S3. Crystallographic parameters of LLNMO-LS.

Cell parameters

Space group: *C2/m*, *a* = 4.9601(2) Å *b* = 8.5694(3) Å, , *c* = 5.0330(5) Å, beta = 109.2480(2)°,

V = 201.9691(7) Å³,

Atomic positions

Name	site	x	y	z	Fract
Li1	2c	0.000	0.000	0.500	1.000
Li2	4h	0.000	0.695	0.500	0.944
Ni2	4h	0.000	0.695	0.500	0.054
Ni1	2b	0.000	0.500	0.000	0.212
Li3	2b	0.000	0.500	0.000	0.416
Mn2	2b	0.000	0.500	0.000	0.380
Mn1	4g	0.000	0.174	0.000	0.710
Ni3	4g	0.000	0.174	0.000	0.140
Li4	4g	0.000	0.174	0.000	0.149
O1	4i	0.210	0.000	0.221	1.000
O2	8j	0.253	0.332	0.227	1.000

Refinement parameters

R_{wp}= 2.43 %, R_p= 1.98 %, χ^2: 1.75

Table S4. A comparison of discharge capacities between LLNMO-LS and other Li-rich cathode materials at high C-rates.

Molecular formula	Voltage window (V)	Electrochemical performance	References
$Li_{1.2}Ni_{0.13}Co_{0.13}Mn_{0.54}O_2$	2.0-4.8 V	147.9 mAh g^{-1} at 5 C 118.3 mAh g^{-1} at 10 C	[1]
$Li_{1.2}Ni_{0.185}Mn_{0.585}Fe_{0.03}O_{1.98}Cl_{0.02}$	2.0-4.8 V	145.6 mAh g^{-1} at 5 C	[2]
$Li[Li_{0.2}Ni_{0.2}Mn_{0.6}]O_2$	2.0-4.8 V	158 mAh g^{-1} at 5 C 131 mAh g^{-1} at 10 C	[3]
$Li[Li_{0.2}Ni_{0.2}Mn_{0.6}]O_2$	2.0-4.8 V	160 mA h g^{-1} at 5 C	[4]
$Li_{1.2}Ni_{0.13}Co_{0.13}Mn_{0.54}O_2$	2.0-4.8 V	125 mAh g^{-1} at 5 C	[5]
LLNMO-LS	2.0-4.8 V	181 mAh g^{-1} at 5 C 147 mAh g^{-1} at 10 C	This work

Table S5. Fitting results of equivalent circuit from Nyquist curves in **Figure 3d** for the electrodes.

Item	LLNMO-L	LLLNMO-LS
R_{ct}	189 Ω	146 Ω
D_{Li^+} (cm^{-2} s^{-1})	2.08×10^{-13}	9.66×10^{-13}

References

1.   B. Chen, B. Zhao, J. Zhou, Z. Fang, Y. Huang, X. Zhu and Y. Sun, *J. Mater. Sci. Technol.*, 2019, **35**, 994-1002.

2.   L. Nie, Z. Wang, X. Zhao, S. Chen, Y. He, H. Zhao, T. Gao, Y. Zhang, L. Dong, F. Kim, Y. Yu and W. Liu, *Nano Lett.*, 2021, **21**, 8370-8377.

3.   A. Zhu, Q. Wang, Y. Zhang, Y. Zhang, X. He, K. Wu, H. Wu, Q. Wang, W. Cai and Y. Zhang, *J. Energy Chem.*, 2022, **71**, 384-391.

4.   J. Sun, X. Cao, W. Yang, E. Yoo and H. Zhou, *J. Mater. Chem. A*, 2023, **11**, 13956-13964.

5.   L. Li, Y. Chen, Y. Liu, Q. Zhang, J. Wu and Q. Yuan, *Rare Metals*, 2023, **42**, 830-837.